POLITECNICO DI TORINO
Repository ISTITUZIONALE

Global/Local Performance Analysis of Driving Force Based Hierarchical Decentralized Motion Control System for Multi-Motor Vehicles

Original
Global/Local Performance Analysis of Driving Force Based Hierarchical Decentralized Motion Control System for Multi-Motor Vehicles / Nguyen, B.-M., Fujimoto, H., Tota, A., Sorniotti, A., Hara, S.. - (2025), pp. 1-6. (51st Annual Conference of the IEEE Industrial Electronics Society, IECON 2025 Madrid (ESP) 14-17 October 2025) [10.1109/IECON58223.2025.11221801].

Availability:
This version is available at: 11583/3008492 since: 2026-03-10T09:37:28Z

Publisher:
IEEE Computer Society

Published
DOI:10.1109/IECON58223.2025.11221801

Terms of use:

This article is made available under terms and conditions as specified in the corresponding bibliographic description in the repository

Publisher copyright
IEEE postprint/Author's Accepted Manuscript

©2025 IEEE. Personal use of this material is permitted. Permission from IEEE must be obtained for all other uses, in any current or future media, including reprinting/republishing this material for advertising or promotional purposes, creating new collecting works, for resale or lists, or reuse of any copyrighted component of this work in other works.

(Article begins on next page)

19 November 2026

Global/Local Performance Analysis of Driving Force Based Hierarchical Decentralized Motion Control System for Multi-Motor Vehicles

Binh-Minh Nguyen,
and Hiroshi Fujimoto
The University of Tokyo
Kashiwa, Chiba, Japan

Antonio Tota,
and Aldo Sorniotti
Polytechnic University of Turin
Turin, Italy

Shinji Hara,

Institute of Science Tokyo
Tokyo, Japan

***Abstract*—Although driving force control (DFC) has been proven to be one of the most promising strategies for traction control, its integration with other motion control functions in electric vehicle (EV) remains an open research challenge. This is because DFC has traditionally been developed utilizing single-wheel-model without consideration for other motion control objectives. To address this limitation, this paper presents a preliminary investigation into a hierarchical decentralized motion control system for multi-motor EVs, based on the DFC. In this architecture, the upper layer is responsible for vehicle speed control, while the lower layer comprises multiple DFC units-treating speed and driving force control are as global and local objectives, respectively. Additionally, a middle layer is to allocate the driving forces to attain supplementary goals. To facilitate a systematic design methodology, a role-sharing mechanism between upper and lower layers is established via a concept of "global/local shared model set." This concept enables both layers to be designed using standard robust control techniques. Notably, the design complexity remains independent of the number of actuators. Using a real in-wheel-motor vehicle, this paper demonstrates-both theoretically and numerically-that the trade-off between global and local objectives can be analyzed through the size of the shared model set.**

Keywords—driving force control, in-wheel-motor, shared model set, robust control, control performance.

I. INTRODUCTION

The remarkable advantages of electric motor has enables the realization of various EV motion control methods since the beginning of this century [1]. In response to the uptrend in the number of motor actuators, particularly in-wheel-motor (IWM), vehicle motion control system would have a hierarchical decentralized architecture [2]. In such architecture, the upper layer is to achieve global motion objectives of vehicle body, such as speed, yaw-rate, side-slip angle. Meanwhile, the lower layer handles traction control by targeting local objectives, such as slip ratio, wheel speed, and driving force. Additional objectives, such as energy optimized torque/force allocation, can be addressed in the middle layer.

However, the aforementioned objectives of upper, middle, and lower layers, have largely been separately studied in literature on EV motion control. For instance, range extension control via front-rear torque distribution [3] was merely studied in isolation, without considering the upper and lower layers. Although torque vectoring control [4] simultaneously attains yaw-rate control and energy-efficient torque distribution, its integration with traction control remains an open question. While an optimal traction control method [5] was developed for multi-IWM-EVs, it merely tackles the local objective of slip ratio. To advance development of EV motion control, the following research question is essential: Can we develop a unified motion control framework that unifies the upper, middle, and lower layers. This question gives raise to two issues: First, can the complexity of system design be reduced, particularly in EVs equipped with multiple motor actuators? Second, can the relationship between performances of the different layers be systematically analyzed?

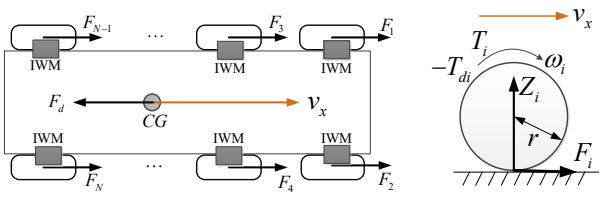
To address the above questions, this paper is motivated by two key ideas: the global/local-shared model set (GL-SMS), and the driving force control (DFC). GL-SMS, proposed by Hara et al., provides a solution for designing hierarchical decentralized control system with aggregation and distribution channels [6]. This concept has been successfully applied to motion control of multi-rotor system, where the global objective is attitude control, and the local objective is propeller speed control [7]. On the other hand, the TMECH article [8] demonstrated that DFC is the most advanced traction control strategies, offering straightforwardly integrated with both middle and upper layers. A recent study [9] further validated the effectiveness of DFC by showing enhanced lateral stability in a hierarchical decentralized control system where DFC is implemented in the lower layer, alongside speed and yaw-rate control in the upper layer.

Thanks to the GL-SMS, this paper establishes a fairly general framework to design hierarchical decentralized motion control for IWM-EVs. The upper layer governs vehicle speed while the lower layer manages driving force at each individual wheel. These layers are interconnected via a driving force aggregation channel which models the longitudinal dynamics of the vehicle body; and a torque distribution channel, which transmits commands from speed controller to force controllers. The proposed design procedure effectively mitigates the complexity associated with the increasing number of motor actuators. Notably, it does not require a complete dynamical model of the entire vehicle system. Although the each controller is designed separately, their performances can be simultaneously analyzed via the GL-SMS volume. Using a real IWM-EV model [8], this paper clarifies the trade-off between speed control and force control.

II. PROBLEM SETTING

A. Vehicle Model

Fig. 1 demonstrates the longitudinal model of an EV driven by N motors. m is the vehicle mass, v_x is the vehicle speed, F_i and F_d represents the driving force and the total resistance force, respectively. J_i and r are the inertia and



(a) Vehicle body. (b) Wheel.

Fig. 1. Longitudinal vehicle model.

radius of the wheel, respectively. T_i is the motor torque, T_{di} is the local disturbance torque, Z_i is the vertical force, and ω_i is the rotational speed of the wheel. The motions of the vehicle body and wheels are given as:

$$m\dot{v}_x = [1\ 1\ \dots\ 1]\mathbf{F} - F_d \tag{1}$$

$$J_i\dot{\omega}_i = T_i - T_{d,i} - rF_i \tag{2}$$

where $\mathbf{F} = [F_1\ F_2\ \dots F_N]^{\mathrm{T}}$. Let ε be a small positive number for preventing division by zero, the slip ratio is defined as:

$$\lambda_i = \frac{r\omega_i - v_x}{\max\{r\omega_i, v_x, \varepsilon\}} \tag{3}$$

We have $F_i = \mu_i(\lambda_i)$, where there exists a nonlinear relationship between road friction coefficient μ_i and slip ratio λ_i, commonly characterized by the magic formula [10].

B. Hierarchcial Decentralized Motion Control System

As shown in Fig. 2, the physical space is to describe the vehicle dynamics. In the lower layer, $P_{l,i}$ is the transfer function from motor torque to driving force, which was derived in [8] and [11]. In the upper layer, $P_g = 1/ms$ is the transfer function from the total of driving force to vehicle speed, which can be derived from (1). The cyber-space consists of the hierarchical decentralized control system. In the lower layer, the force controller $C_{l,i}$ might have the single loop configuration [8] or cascade configuration [11]. In the upper layer, C_g is the transfer function of the vehicle controller, which outputs the total driving force command F^*_{all}. This command is distributed to lower layer as $F^*_i = k_i F^*_{all}$. In

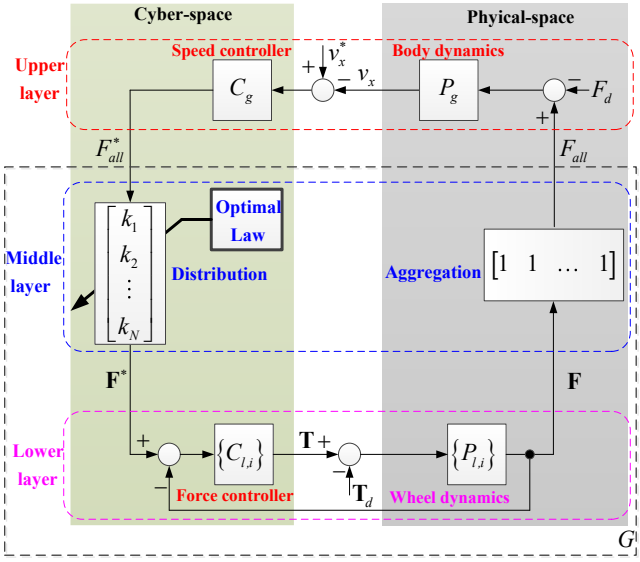


Fig. 2. Hierarchical decentralized motion control system.

the middle layer, an optimal law, such as workload minimization and or energy minimization, can be implemented to determine $\{k_i\}$ in real time [2][3][4]. The optimization also has to satisfy some constraints, such as the generation of yaw moment. Especially, the following constraint must be maintained: $k_1 + k_2 + \cdots + k_N = 1$. Since this paper focuses on control performance analysis, the optimization algorithm—being outside the main scope—is not discussed. In Fig. 2, the vectors of size N are defined as:

$$\mathbf{F} = [F_1\ F_2\ \dots\ F_N]^{\mathrm{T}}, \mathbf{F}^* = [F_1^*\ F_2^*\ \dots\ F_N^*]^{\mathrm{T}}$$

$$\mathbf{T} = [T_1\ T_2\ \dots\ T_N]^{\mathrm{T}}, \mathbf{T}_d = [T_{d,1}\ T_{d,2}\ \dots\ T_{d,N}]^{\mathrm{T}}$$

Remark 1: In the DFC strategy [8] and [11], the feedback of F_i is implemented via a Driving Force Observer (DFO), designed based on (2). Since this paper focuses on performance analysis, the DFO is preliminarily omitted for simplicity of block diagram. However, the time constant of the DFO can be lumped into the local dynamics of $P_{l,i}$.

III. Proposed Global/Local Design

With respect to the problem setting in the previous section, the system in Fig. 2 can be designed via the following procedure.

Step 1 (Selection of GL-SMS): The nominal transfer function of the local subsystem is $G_n = P_{ln}C_{ln}/(1 + P_{ln}C_{ln})$, where P_{ln} is the nominal representative of $\{P_{l,i}\}$, and C_{ln} can be obtained by pole placement to G_n. It should be noted that, if the selected poles are too small, the control performance of the nominal model is poor. On the other hand, if the poles are too large, vibration might happen. This is due to the fact that the in-wheel-motor has a certain maximum torque. The GL-SMS is defined as $\{G_n, \delta\}$ where the volume $\delta \in (0,1)$.

Step 2-L (Local design): Each local controller $C_{l,i}$ is designed to satisfy a couple of conditions:

(i) Local control performance:

$$\left\|\sigma_{l,i}S_{l,i}\right\|_\infty \le 1,\ S_{l,i} = \frac{P_{l,i}}{1 + P_{l,i}C_{l,i}} \tag{4}$$

where $S_{l,i}$ is the sensitivity function from the local disturbance $T_{d,i}$ to the local driving force, and $\sigma_{l,i}$ represents the local performance index.

(ii) Modeling matching condition:

$$\left\|\Delta_{l,i}\right\|_\infty = \left\|\frac{G_{l,i} - G_n}{G_n}\right\|_\infty \le \delta,\ G_{l,i} = \frac{P_{l,i}C_{l,i}}{1 + P_{l,i}C_{l,i}} \tag{5}$$

where $G_{l,i}$ is the transfer function from F^*_i to F_i.

Step 2-G (Global design): Designing the local subsystem to satisfy (5), the transfer function from F^*_{all} to F_{all} becomes:

$$G = \sum_{i=1}^{N} k_i G_{l,i} = \sum_{i=1}^{N} k_i G_n\left(1 + \Delta_{l,i}\right) = G_n\left(1 + \Delta_l\right) \tag{6}$$

Since the summation of $\{k_i\}$ equals to 1, it can be shown from (5) that the following inequality holds true:

$$\left\|\Delta_l\right\|_\infty = \left\|\sum_{i=1}^{N} k_i \Delta_{l,i}\right\|_\infty \le \delta \tag{7}$$

In other word, G can be treated as G_n with the multiplicative error Δ_l bounded by the volume of the nominal model set. Thus, the global controller can be designed by the block diagram shown in Fig. 3a. To analyze stability and performance, we equivalently expressed it as in Fig. 3b with the two-by-two block φ:

$$\varphi = \frac{1}{1+P_g C_g G_n}\begin{bmatrix} -P_g & P_g \\ P_g C_g G_n & -P_g C_g G_n \end{bmatrix} = \begin{bmatrix} \varphi_{11} & \varphi_{12} \\ \varphi_{21} & \varphi_{22} \end{bmatrix} \tag{8}$$

In Fig. 3b, the virtual perturbation is introduced as $\left\|\Delta_p\right\|_\infty \le \sigma_g$, where σ_g represents the global performance index. By scaling, Fig. 3b is equivalently expressed as Fig. 3c with the two-by-two block:

$$\tilde{\varphi} = \begin{bmatrix} \delta^{-1}\sigma_g \varphi_{11} & \delta^{-1}\sigma_g \varphi_{12} \\ \varphi_{21} & \varphi_{22} \end{bmatrix} = \begin{bmatrix} \tilde{\varphi}_{11} & \tilde{\varphi}_{12} \\ \tilde{\varphi}_{21} & \tilde{\varphi}_{22} \end{bmatrix} \tag{9}$$

From (7) and the setting of Δ_p, the perturbation in Fig. 3c is also bounded by the volume of GL-SMS:

$$\left\|\Delta_{\tilde{\varphi}}\right\|_\infty = \left\|diag\left\{\delta\sigma_g^{-1}\Delta_p, \Delta_l\right\}\right\|_\infty \le \delta \tag{10}$$

Following the μ-synthesis theory [12], the condition for the upper layer to be well-posed and internally stable is:

$$\sup_{\omega} \mu_{\Delta_{\tilde{\varphi}}}\left(\tilde{\varphi}(j\omega)\right) \le \delta^{-1} \tag{11}$$

Remark 2: Thanks to the GL-SMS, each controller $\{C_{l,i}, C_g\}$ can be designed separately from the others. This strategy remarkably alleviates the design burden, as it is not essential to derived the entire dynamical equations of the system in Fig. 2, which is transparently multi-input multi-output (MIMO). In addition, the design conditions (4), (5) and (11) show that both the local and global performance can be adjusted via the GL-SMS volume.

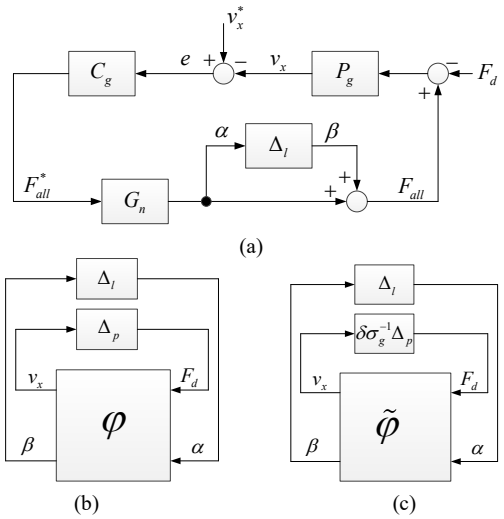


Fig. 3. Upper layer representation using GL-SMS.

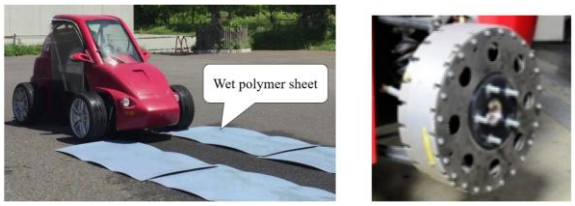


Fig. 4. Experimental EV with IWM actuator.

TABLE I. VEHICLE SPECIFICATION

Vehicle mass m	880 kg
Wheelbase l	1.715 m
Distance from center of gravity to front/rear axles l_f, l_r	1.013 m
	0.702 m
Center of gravity height	0.51 m
Front wheel inertia $J_{1,2}$	1.24 Nm^2
Rear wheel inertia $J_{3,4}$	1.26 Nm^2
Wheel radius r	0.302 m

IV. ILLUSTRATIVE EXAMPLE

A. Case of Study

To clarify the proposed procedure, this paper utilizes the four wheel EV in Fig. 4, which has been used by the authors' research group for vehicle motion control studies [3][8][11]. The basic parameters of the vehicle are summarized in TABLE I. This paper adopts the single loop DFC strategy [11], which normalizes the local transfer function as:

$$P_{l,i} = \frac{a_i}{b_i s + 1},\ a_i = \frac{1}{r + \dfrac{J_i}{r m_i\left(1-\lambda_n\right)}} \tag{12}$$

where b_i represents the lumped time-constant of DFO and motor drives. The mass m_i represents the portion of load on the ith wheel in the static status, and it can be calculated from the distances $l_{f,r}$ in TABLE I. Besides, λ_n is the nominal slip ratio, which can be selected as a small value, such as 0.01. In this paper, the local dynamics parameters are calculated as $a_{1,2} = 0.29^{-1}[m^{-1}]$, $a_{3,4} = 0.31^{-1}[m^{-1}]$, $b_{1,2} = 0.102\ [s]$, $b_{3,4} = 0.112[s]$. It is possible to select the proportional integral (PI) controller for both the upper and lower layers:

$$C_{l,i} = \frac{K_{P,i}s + K_{I,i}}{s}, C_g = \frac{K_{Pg}s + K_{Ig}}{s} \tag{13}$$

B. Derivation of Control Performances

Substitute (12) and (13) into (4) and let $s = j\omega$ (ω denotes the frequency term, and it is different to the wheel speed ω_i), the condition of the local performance becomes:

$$\sigma_i \sqrt{\frac{a_i^2\omega^2}{\left(a_i K_{I,i} - b_i\omega^2\right)^2 + \left(1 + a_i K_{P,i}\right)^2\omega^2}} \le 1$$
$$\Leftrightarrow \sigma_{l,i}^2 \le \frac{1}{a_i^2}\left[\begin{matrix}\left(1+a_i K_{P,i}\right)^2 - 2a_i b_i K_{I,i} \\ +b_i^2\omega^2 + \dfrac{a_i^2 K_{I,i}^2}{\omega^2}\end{matrix}\right], \forall\omega > 0 \tag{14}$$

Let $X = \omega^2$, (14) is rewritten as:

$$\sigma_{l,i}^2 \le f_i(X) = A_i + B_i X + \frac{C_i}{X} \ \forall X > 0 \qquad (15)$$

where $A_i = \frac{\left(1 + a_i K_{P,i}\right)^2 - 2a_i b_i K_{I,i}}{a_i^2}, B_i = \frac{b_i^2}{a_i^2}, C_i = K_{I,i}^2$.

Solving $\partial f_i(X)/\partial X = 0$, the minimum value of $f_i(X)$ is:

$$\min_{X>0} f_i(X) = A_i + 2\sqrt{B_i C_i} = \frac{\left(1 + a_i K_{P,i}\right)^2}{a_i^2} \qquad (16)$$

Thus, the optimal local control performance index is

$$\sigma_{l,i}^* = \frac{1 + a_i K_{P,i}^*}{a_i} \qquad (17)$$

where $K_{P,i}^*$ is the maximum proportional gain that satisfies the model matching condition (5) with a given volume of the shared model set.

Next, we derive the global control performance. As it is very complex to calculate the μ-value directly, a standard scheme is to approximate the μ-value by its upper-bound. Considering the two-by-two block of the upper layer in Fig.3c, the following inequality is obtained [12]:

$$\mu_{\Delta_\varphi}\left(\tilde{\varphi}(j\omega)\right) \le \sqrt{\left|\tilde{\varphi}_{11}\right|^2 + \left|\tilde{\varphi}_{12}\right|^2 + \left|\tilde{\varphi}_{21}\right|^2 + \left|\tilde{\varphi}_{22}\right|^2} \qquad (18)$$

Substitute the upper-bound (18) into (11), we have:

$$\sigma_g^2 \le f_g(\omega) = \frac{1 - \delta^2\left(\left|\varphi_{21}\right|^2 + \left|\varphi_{22}\right|^2\right)}{\left|\varphi_{11}\right|^2 + \left|\varphi_{12}\right|^2}, \forall \omega > 0 \qquad (19)$$

Thus, the global control performance can be approximated as follows:

$$\sigma_g^* = \sqrt{\min_{\omega} f_g(\omega)\Big|_{K_{Pg}=K_{Pg}^*, K_{Ig}=K_{Ig}^*}} \qquad (20)$$

where $\{K_{Pg}^*, K_{Ig}^*\}$ is the solution of the optimization problem:

$$\max_{\{K_{Pg}, K_{Ig}\}} \min_{\omega} f_g(\omega) \qquad (21)$$

Remark 3: The inequality (19) indicates that increasing the volume of the GL-SMS leads to a deterioration in global control performance. This is because a larger volume δ introduces greater perturbation to the upper layer block. On the other hand, increasing δ relaxes the model matching condition (5), which may allow for a larger optimal proportional gain in (17), thereby, enhancing the local control performance. In summary, a trade-off exists between global and local control performances. Therefore, the volume of the GL-SMS should be carefully selected to design the hierarchical decentralized motion control system for EVs.

C. System Design using the Proposed Procedure

Applying the analysis in the previous sub-section, we design the controllers for the EV shown in Fig. 4.

Step 1: The nominal model is selected as:

$$P_{ln} = \frac{a_n}{b_n s + 1} = \frac{0.3^{-1}}{0.107 s + 1} \qquad (22)$$

Placing the poles of the close loop system including P_{ln} and C_{ln} at the stable value $-\rho_n = -10$, we have:

$$C_{ln} = \frac{K_{Pn} s + K_{In}}{s} = \frac{\left(2b_n\rho_n - 1\right)s + b_n\rho_n^2}{a_n s} \qquad (23)$$

Step 2-L: Similarly, by placing the pole of the local subsystem at the stable value $-\rho_i$, the local controller is:

$$C_{l,i} = \frac{K_{P,i} s + K_{I,i}}{s} = \frac{\left(2b_i\rho_i - 1\right)s + b_i\rho_i^2}{a_i s} \qquad (24)$$

Substitute (12), (22), (23) and (24) into (5), the model matching condition becomes:

$$\left\| \frac{\frac{\left(2b_i\rho_i - 1\right)s + b_i\rho_i^2}{b_i\left(s + \rho_i\right)^2} - \frac{\left(2b_n\rho_n - 1\right)s + b_n\rho_n^2}{b_n\left(s + \rho_n\right)^2}}{\frac{\left(2b_n\rho_n - 1\right)s + b_n\rho_n^2}{b_n\left(s + \rho_n\right)^2}} \right\|_\infty \le \delta \qquad (25)$$

Solving (25) with diffrent values of the GL-SMS volume, we obtained in TABLE II the maximum allowable ρ_i^*, and consequently the maximum proportional gain $K_{P,i}^*$. As our hypothesis in the previous sub-section, the maximum proportional gains $K_{P,i}^*$ of the local controller is increased by increasing δ.

TABLE II. VEHICLE SPECIFICATION

Volume δ	**Max poles $\rho_{1,2}^*$**	**Max P gain $K_{P,1,2}^*$**	**Max poles $\rho_{3,4}^*$**	**Max P gain $K_{P,3,4}^*$**
0.1	10.76	0.3466	10.32	0.4066
0.2	11.29	0.3779	10.85	0.4434
0.3	11.83	0.4099	11.39	0.4809
0.4	12.36	0.4412	11.92	0.5177
0.5	12.89	0.4726	12.46	0.5552
0.6	13.43	0.5045	12.99	0.5920
0.7	13.96	0.5395	13.52	0.6288
0.8	14.49	0.5672	14.05	0.6656
0.9	15.02	0.5986	14.59	0.7031

Step 2-G: Placing the poles of the close loop system including P_g and C_g are placed at the stable value $-\rho_g$, the global controller is obtaine as:

$$C_g = \frac{K_{Pg}s + K_{Ig}}{s} = \frac{2m\rho_g s + m\rho_g^2}{s} \tag{26}$$

From (22) and (23), we have:

$$G_n = \frac{P_{ln}C_{ln}}{1 + P_{ln}C_{ln}} = \frac{(2b_n\rho_n - 1)s + b_n\rho_n^2}{b_n(s+\rho_n)^2} \tag{27}$$

Substitute (26) and (27) into (8), we have:

$$\varphi_{11} = -\varphi_{12} = \frac{-b_n s(s+\rho_n)^2}{L(s)} \tag{28}$$

$$\varphi_{21} = -\varphi_{22} = \frac{(2m\rho_g s + m\rho_g^2)\left[(2b_n\rho_n - 1)s + b_n\rho_n^2\right]}{L(s)} \tag{29}$$

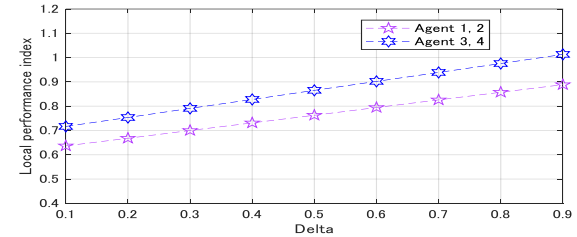
where

$$L(s) = mb_n s^2(s+\rho_n)^2 + (2m\rho_g s + m\rho_g^2)\left[(2b_n\rho_n - 1)s + b_n\rho_n^2\right]$$

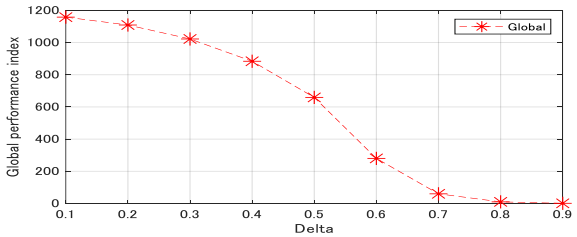
In practical applications, any electric vehicle has a certain maximum driving force/torque. Thus, the value of ρ_g should not be too big to prevent the system from fluctuation. In many scenarios, ρ_g is about 10% of $\rho_{l,i}$ and must not be bigger 20% of $\rho_{l,i}$. Hence, we substitute (28) and (29) into (19) and (21), and perform the following optimization problem:

$$\max_{\{\rho_g\}} \min_{\omega} f_g(\omega), \text{ with } \rho_g \in (0,2) \tag{30}$$

Based on the results in TABLE II and the optimization (30), the global and local control performances are plotted in Fig. 5. Transparently, the global and local performances exhibit a trade-off, where the global performance decreases and the local performance increases monotonically with respect to the GL-SMS volume. To compromise such trade-off, a reasonable approach is to select the GL-SMS volume within a middle-range, such as from 0.2 to 0.4.



(a) Local.



(b) Global.

Fig. 5. Global and local control performances.

D. Simulation Evaluation

To validate the theoretial discussion in sub-section IV-B and numerical analysis in sub-section IV-C, a vehicle simulator was established using Matlab/Simulink and the parameters listed in TABLE I. Three test cases were conducted with different selection of the model set volume to design the controllers:

Case 1 (Small delta): The GL-SMS volume is $\delta = 0.1$.

Case 2 (Medium delta): The GL-SMS volume is $\delta = 0.4$.

Case 3 (Big delta): The GL-SMS volume is $\delta = 0.8$.

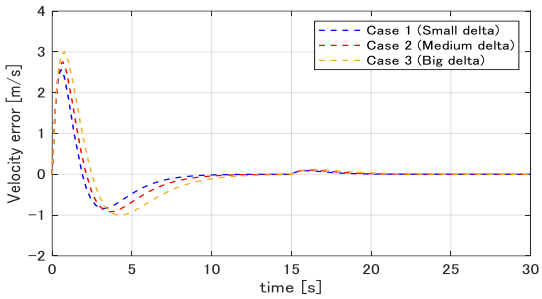
The vehicle is accelerated from 0 to 10 m/s over the first 5 seconds and then maintains this speed until 30 seconds. At 15 seconds, a global disturbance is inputted to the system to simulate a sudden change in the road slope and/or wind conditions. The driving force command F_{all}^* is equally distributed to each wheel with the distribution ratios set as $k_i = 0.25, \forall i \in [1,4]$.

To investige the control performances, the tracking errors of the vehicle speed (global) and the driving force (local) are presented in Figs. 6 and 7, respectively. Since the driving forces are equally distributed to all wheels, their local results are nearly the same. Therefore, only the results of the first wheel are shown. Fig. 6a illustrates that increasing the volume of the GL-SMS leads to a larger tracking error between the vehicle velocity and its reference. This also "amplifies" the impact of the global disturbance on the velocity tracking error, as shown in Fig. 6b. In contrast, Fig. 7a indicates that a larger GL-SMS volume results in a smaller tracking error between the driving force and its reference. Consequently, the influence of global disturbances on the driving force tracking error is mitigated, as demonstrated in Fig. 7b.

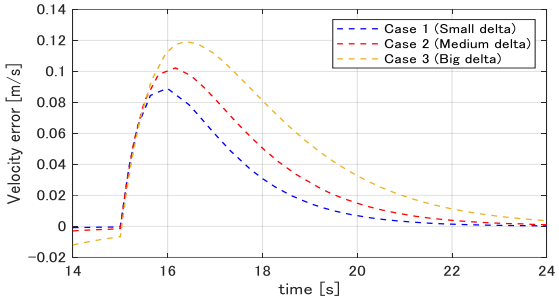
In summary, the simulation results are consistent with the theoretical analysis presented in Fig. 5. The trade-off between the global and local control performances is clearly demonstrated. Among these cases studied, Case 2-with a medium volume of the GL-SMS- emerges as a reasonable candidate for hierarchical decentraized motion control system. The corresponding results, including the vehicle speed and driving force of the first wheel, are illustrated in Fig. 8.

V. Conclusions

This paper preliminary establishes a general framework for hierarchical motion control system of EVs, based on driving force control at each local wheel. The proposed approach introduces the concept of global/local-shared model as the core theoretical foundation for designing the control system in the context of robust stability. Notably, the complexity and computational cost of the proposed design procedure are independent of the number of motor actuators. Furthermore, the control performances can be systematically analyzed through the volume of the shared model set, enabling a structured method to tune and coordinate the upper- and lower-layer controllers. In future, the proposed framework will be validated via real-time experiments. Additional control objectives, such as torque vectoring control and energy optimization, will also be integrated. The cascade driving force controller will be investigated as a promising configuration for the lower-layer control system.

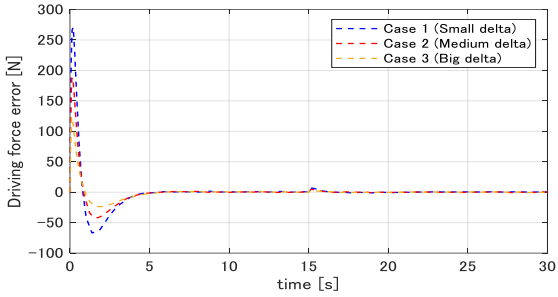


(a) Overall results.

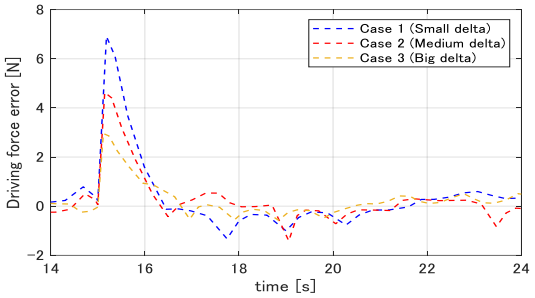


(b) The period under global disturbance.

Fig. 6. Global performance: Tracing error of vehicle speed.

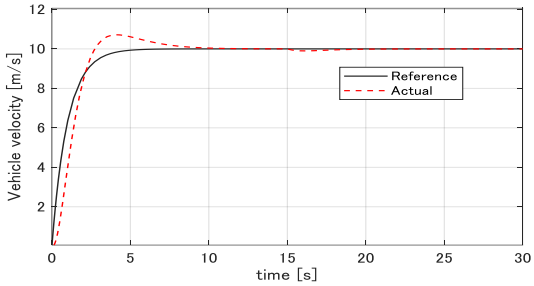


(a) Overall results.



(b) The period under global disturbance.

Fig. 7. Local performance: Tracing error of driving force.



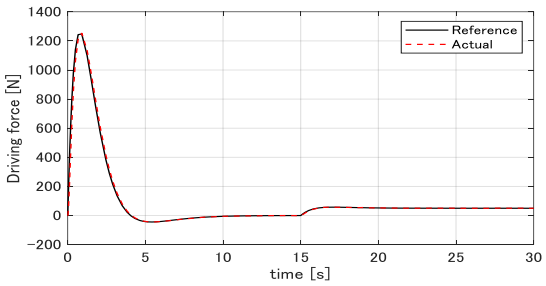


Fig. 8. Results of Case 2 with medium GL-SMS volume.

ACKNOWLEDGMENT

This work was supported by JSPS Kakenhi Grant Number 25K07790 and the Nagamori Grant for Young Researcher.

REFERENCES

[1] Y. Hori, “Future vehicle driven by electricity and control-Research on four-wheel-motored ‘UOT Electric March II’,” IEEE Transactions on Industrial Electronics, vol. 51, no. 5, pp. 954-962 (2004).

[2] B.-M. Nguyen et al., “Longitudinal motion control of electric vehicles: Glocal model and design using passivity,” IEEE Vehicular Technology Magazine, vol. 16, no. 3, pp. 75-86 (2021).

[3] H. Fujimoto and S. Harada, “Model based range extension control system for electric vehicles with front and rear driving-braking force distribution,” IEEE Transactions on Industrial Electronics, vol. 62, no. 5, pp. 3245-3254 (2015).

[4] G. De Filippis et al., “Energy-efficient torque-vectoring control of electric vehicles with multiple drivetrains,” IEEE Transactions on Vehicular Technology, vol. 67, no. 6, pp. 4702-4715 (2018).

[5] B.-M. Nguyen et al., “Slip control for IWM vehicles based on hierarchical LQR,” Control Engineering Practice, vol. 93, no. 104179 (2019).

[6] S. Hara et al., “Hierarchically decentralized control for networked dynamical systems with global and local objectives,” in: R. Tempo, S. Yurkovich, P. Misra (eds): “Emerging applications of control and systems theory: Lecture notes in control and information sciences,” (2018).

[7] B. M. Nguyen et al., “Disturbance observer-based global/local control using shared model set: Design concept with practical application to multi-rotors,” IEEJ Journal of Industry Applications, vol. 14, no. 3, pp. 431-441 (2025).

[8] T. Ueno et al., “Wheel velocity based cascade driving force control for electric vehicles,” IEEE/ASME Transactions on mechatronics, Early Access, doi: 10.1109/TMECH.2024.3456151 (2024).

[9] S. Sato, “Sideslip angle based variable slip ratio limiter for direct yaw moment control of two-input two-outpu motor vehicles,” IEEE International Conference on Advanced Intelligent Mechatronics, pp. 1476-1481 (2024).

[10] H. Pacejka and I. J. M. Besselink, “Tire and vehicle dynamics,” Butterworth-Heinemann (2012).

[11] J. Amada and H. Fujimoto, “Torque based direct driving force control method with driving stiffness estimation for electric vehicle with in-wheel-motor,” 38th Annual Conference on IEEE Industrial Electronic Society, pp. 4904-4909 (2012).

[12] K. Zhou and J. C. Doyle, “Essentials of Robust Control,” Prentice-Hall (1998).